SLAC-PUB-2467
February 1980
(T/E)

PHASE AND ENERGY CORRECTING INELASTIC CONTRIBUTIONS IN MULTIPLE RESCATTERING*

R. W. B. Ardill and K. J. M. Moriarty
Royal Holloway College
Englefield Green, Egham, Surrey TW20 0EX, UK

Peter Koehler
Stanford Linear Accelerator Center
Stanford University, Stanford, California 94305

Abstract: In this paper we modify the phase and energy behaviour of conventional weak cut absorption. We parameterize the double scattering amplitude of the Regge-Gribov scheme to include low and high mass inelastic intermediate states. This is done through the introduction of azimuthal correlations between the Reggeon and the regular Pomeron and reverses the anticlockwise rotation induced by absorptive cuts. For precision we include Regge-Regge cuts and achieve accurate fits to the vector and tensor amplitude analysis at 6 GeV/c. Polarization and line-reversal symmetry-breaking deficiencies in charge and hypercharge exchange processes are thus remedied at this energy. Crossover and polarization show a very weak dependence against variations over a wide range of energy. Inelastic and elastic polarization of πN scattering are reconciled for $|t| \gtrsim \alpha_\rho = 0$. The clockwise rotation included in isoscalar exchange arranges for rising cross sections without assuming $\alpha_p(0) > 1$.

Submitted to Il Nuovo Cimento A

* Work supported by the Department of Energy, contract DE-AC03-76SF00515.

1. Introduction

Gribov's Reggeon Calculus ([1]) is the only known theory of soft hadronic two-body reactions. It is based on the consistent implementation of multiperipheral ideas and unitarity. Through unitarity colliding hadrons become extended objects and form virtual constituents in a cascade of decays. The corresponding constitutents of both hadrons interact causing the simultaneous production of multiperipheral showers, which in turn correspond to Reggeons. The Reggeons scatter with the external hadrons in the same way as ordinary particles. S-channel unitarity is thus manifested in the Reggeon particle scattering amplitude through the presence of inelastic intermediate states. A variety of cut prescriptions can be extracted, among them eikonal cuts ([2]) and their derivatives ([3,4]) and pole-enhanced cuts ([5,6,7]) The latter produce the energy dependence of differential cross sections. However, eikonal and pole-enhanced cuts possess only elastic pole singularities and give incorrect phases, manifested in polarization deficiencies. To overcome this we parameterize the inelastic low mass intermediate states, and then combine with the elastic pole singularities to achieve more subtle phase effects.

We would emphasize that it is the false assumption of independent rescattering adopted in conventional eikonal models which is responsible for the poor description of the helicity nonflip vector and tensor phases.

(1) M. Baker and K. A. Ter-Martirosyan, Phys. Rev. 28C (1976) 1.
(2) K. A. Ter-Martirosyan, Sov. Journ. Nucl. Phys. 10 (1970) 600.
(3) K. G. Boreskov et al., Sov. Jour. Nucl. Phys. 14 (1972) 457.
(4) Sh. S. Eremyan, Sov. Journ. Nucl. Phys. 21 (1975) 195.
(5) K. A. Ter-Martirosyan, Sov. Journ. Nucl. Phys. 10 (1970) 715.
(6) Bipin A. Desai and P. R. Stevens, Phys. Rev. D11 (1975) 2449.
(7) P. D. B. Collins and A. Fitton, Nucl. Phys. B91 (1975) 332.

We parameterize by introducing azimuthal correlations between Pomeron and regular Reggeon. We use a correlation modified exponential which includes the mutual orientation of the Reggeon transverse momenta. This is more general than the elastic Gaussian model adopted in eikonal cuts. We thus introduce a new element in cut models: a correlation parameter c which governs a $|t|$-dependent modified cut phase and a corresponding cut strength, both sensitive to exchange and helicity. We find that the correlation parameter c of the helicity nonflip vector and tensor amplitudes is real and negative in the presence of a moving Pomeron pole.

2. Formalism

We represent the amplitudes as vectors in the complex plane

$$T^{0,1}_{R,el,C,tot,exp}(|t|) = \left|T^{0,1}(|t|)\right| \exp\left[i\phi^{0,1}(|t|)\right] ,$$

R = Reggeon, i.e., the ρ, A_2, f, P

el = elastic amplitude

tot = total theoretical amplitude obtained as sum of pole and cut

exp = amplitude as extracted by amplitude analysis ([8,9])

0,1 indicate helicity nonflip and helicity flip, respectively.

A. The ρ, A_2 Regge Pole Amplitude

The modulus of the helicity nonflip pole amplitude at fixed s is parameterized (assuming the presence of nonsense wrong signature zero

(8) I. Ambats et al., Phys. Rev. 9D (1974) 1179.
(9) G. Girardi et al., Nucl. Phys. B76 (1974) 541; G. Girardi and H. Navelet, Nucl. Phys. B83 (1974) 377.

(NWSZ) for the ρ as

$$\left|T^0_{\rho=R}(|t|)\right| = 2\beta^0_R(0)\ \sin\left\{\tfrac{1}{2}\pi\left(\alpha_R(0) - \alpha'_R|t|\right)\right\} \cdot \exp\left[-\lambda^0_R|t|\right],$$

and for the A_2 as

$$\left|T^0_{A_2=R}(|t|)\right| = 2\beta^0_R(0)\cos\left\{\tfrac{1}{2}\pi\left(\alpha_R(0) - \alpha'_R|t|\right)\right\}\exp\left[-\lambda^0_R|t|\right],$$

with $\beta^0_R(0)$ the residue in forward direction; λ^0_R the slope of the assumed exponential fall-off of the residue and $\alpha_R(0)$ and α'_R intercept and slope, respectively, of the linear Regge trajectory.
(Parameter values are in Table 1.)

The point $\alpha_{R=A_2} = 0$ which was a wrong signature point for the ρ is now a right signature point. Thus there is no zero in the Regge pole amplitude at $\alpha_{R=A_2} = 0$.
The Regge phase, rising linearly, is then

$$\phi^0_R(|t|) = \phi^0_R(0) + \Phi^0_R|t|,$$

with an initial phase angle for the ρ and A_2 of

$$\phi^0_R(0) = \tfrac{1}{2}\pi\alpha_R(0) = 43.20^\circ \text{ and } -27^\circ$$

and a rotation velocity of the angle per $|t|$ of

$$\Phi^0_R = \tfrac{1}{2}\pi\alpha'_R = 72.36^\circ \text{ and } 67.5^\circ .$$

B. The Elastic Amplitude

We use a helicity-conserving elastic amplitude and parameterize with one exponential. It has a complex radius of interaction

$$T^{*0}_{el}(|t|) = \beta^{*0}_{el}(0)\ \exp\left[i\delta^{*0}_{el}\right]\ \exp\left[-\lambda^{*0}_{el}|t|\right],$$

where the modulus $\beta_{el}^{*0}(0)$ and the phase δ_{el}^{*0} are real while the radius of interaction λ_{el}^{*0} is complex due to the Regge-like $|t|$-dependent phase $\alpha_{el}^{*\prime} \neq 0$ such that

$$\mathrm{Im}(\lambda_{el}^{*0}) = -\tfrac{1}{2}\pi\alpha_{el}^{*\prime} \quad \text{and} \quad |\lambda_{el}^{*0}|$$

is approximately determined from the observed slope of the elastic scattering.

$$\beta_{el}^{*0}(s) = \tfrac{1}{2}\pi^{-\frac{1}{2}}\sigma_{tot}(s)$$

and δ_{el}^{*0} is the effective initial phase angle of the full elastic amplitude. The final values of β_{el}^{*0}, δ_{el}^{*0} and λ_{el}^{*0} are obtained from amplitude analysis ([8]) at 6 GeV/c. The * indicates that the elastic amplitude is obtained as

$$T_{el}^{*} = f + P + f \otimes P + P \otimes P \ .$$

C. The Double Scattering Amplitude

Our correlation modified cut stands effectively for Gribov's full double scattering amplitude ([5]).

$$T_{ab}^{(2)}(s,\underline{k}) = \frac{i}{\pi}\int_{-\infty}^{\infty} \cdot N(\underline{k}_a,\underline{k}_b,\underline{k},s)\ \delta^2(\underline{k}_a+\underline{k}_b-\underline{k})\ d^2\underline{k}_a\ d^2\underline{k}_b$$

$$\times\ \eta_a\eta_b\ (s/s_0)^{\alpha_a(\underline{k}_a)+\alpha_b(\underline{k}_b)-2}\ ,$$

$$= \frac{i}{\pi}\int_{s_1 t}^{\infty} \cdot (s_0 ds_1)/\pi s_1 \int_{s_2 t}^{\infty} \cdot (s_0 ds_2)/\pi s_2 \int_{-\infty}^{\infty} \cdot \delta^2(\underline{k}_a+\underline{k}_b-\underline{k})$$

$$\times\ d^2\underline{k}_a\ d^2\underline{k}_b \cdot \mathrm{disc}\ F_1(\underline{k}_a,\underline{k}_b,\underline{k},s_1)\ \mathrm{disc}\ F_2(\underline{k}_a,\underline{k}_b,\underline{k},s_2)$$

$$\cdot\ \eta_a(\underline{k}_a)\ \eta_b(\underline{k}_b)\ (s/s_0)^{\alpha_a(\underline{k}_a)+\alpha_b(\underline{k}_b)-2}\ ,$$

$\underline{k}_a$ and $\underline{k}_b$ with $k_{a,b}^2 = |t_{a,b}|^2 = -t_{a,b}$ are the two dimensional Reggeon momenta and $k^2 = (\underline{k}_a+\underline{k}_b)^2 = |t|$ is the total momentum transfer.

The linear Reggeon trajectories are $\alpha_{a,b} = \alpha_{a,b}(0) - \alpha'_{a,b} k^2$. The energy scale is set $s_0 = 1$ GeV. η_a, η_b are the signature factors

$$\eta_{a,b}(\underline{k}_{a,b}) = i\sigma_{a,b} \frac{\exp\left[i\frac{1}{2}\pi\left(\frac{\sigma_{a,b}+1}{2} - \alpha_{a,b}(\underline{k}_{a,b})\right)\right]}{\cos\frac{1}{2}\pi\left(\frac{\sigma_a+1}{2} - \alpha_{a,b}(\underline{k}_{a,b})\right)} \quad ,$$

where

$$\sigma_{a,b} = \pm 1 \quad .$$

The Gribov vertex N factorizes into $N_1 \cdot N_2$. These are the absorptive parts of the Reggeon-particle scattering amplitudes F_1 and F_2.

$$N_{1,2} = \int_{-\infty}^{\infty} F_{1,2}(\underline{k}_a, \underline{k}_b, \underline{k}, s_{1,2}) \frac{ds_{1,2}}{2\pi i s_{1,2}}$$

$$= \int_{s_{1,2}^t}^{\infty} \text{disc } F_{1,2}(\underline{k}_a, \underline{k}_b, \underline{k}, s_{1,2}) \frac{ds_{1,2}}{\pi s_{1,2}} \quad ,$$

where $s_{1,2}$ are the subenergies and $s_{1,2}^t$ the threshold values. The subenergy planes s_1 and s_2 are divided into low and high mass regions such that $s_{1,2} < M^2$ and $s_{1,2} > M^2$, respectively. A special low mass unenhanced diagram where $s_1 < M^2$ and $s_2 < M^2$ is Gribov's high energy approximation of the Mandelstam cut.

With the high mass region taking on its Reggeon behaviour, the full amplitude splits into four parts [5] These are unenhanced (fig. 1a), semi-enhanced (fig. 1b, 1c) and fully enhanced (fig. 1d) diagrams. Here the low mass and the triple Reggeon couplings are depicted as non-planar.

Our two body cut amplitude takes account of low and high mass inelastic intermediate states in the vertex N of Gribov's full double scattering amplitude. The traditional eikonal or absorption model ([2]) is based on a Gaussian form of the Gribov vertex $N(\underline{k}_a, \underline{k}_b)$ and allows only for the elastic intermediate state. The quasi-eikonal model allows for the formation of low mass showers in the intermediate states after each rescattering. The showers enhance the cut strength for elastic scattering at forward direction by a constant factor. The phase and energy behaviour, however, suggest a more subtle parameterization of N. The vertex N has to depend on the angle between $\underline{k}_a$ and $\underline{k}_b$. Since the high mass peripheral nonelastic intermediate states are Regge-approximated, N also has to depend on s. This leads to the diagrams in fig. 1.

The sum of these diagrams gives the cut a pole-like shrinkage at high energy, with the enhanced diagrams b, c and d at rising energies taking the lead over the unenhanced diagram a. Thus, the Gribov vertex N is parameterized as

$$N(\underline{k}_a, \underline{k}_b, \underline{k}, s) = \lambda_{cut}(\underline{k})\ \beta_R(s)\ \beta_P(s) \times \exp\left[-(c_1 + c_2\ \ell n\ s)(\underline{k}_1 - \underline{k}_2)^2 - \lambda_R(s)k_1^2 - \lambda_p(s)k_2^2 \right]$$

D. The Correlation Modified Cut Amplitude

We convolute pole and elastic amplitude by introducing the correlation kernel $K\left(c^0(\ell n\ s)\right)$. We write down the s-channel helicity

sum over the Gribov cut integral for the process A + B → A' + B' (fig. 1)

$$T_{cut}^{m(p)}(s,\underline{k}^2) = \sum_{\mu_1\mu_2} T^{m(p),\mu_1\mu_2}(s,\underline{k}^2)$$

$$= \sum_{\mu_1\mu_2} (i/2\pi^{\frac{3}{2}}) \int_{-\infty}^{\infty} d^2\underline{k}_1 \; d^2\underline{k}_2 \; T_R^{\mu 1}(s,\underline{k}_1^2) \; T_P^{\mu 2}(s,\underline{k}_2^2)$$

$$\times K^{m(p)}(s,\underline{k}_1,\underline{k}_2,\underline{k}) \; \delta^2(\underline{k} - \underline{k}_1 + \underline{k}_2)$$

The helicity sum splits into net helicity nonflip and net helicity flip indicated by m(p) as a function of the individual helicities μ_i (i = 1,2) carried by the exchanged Reggeons. They take on the values 0,1, and $p = \sum_i \mu_i$ defines the net helicity such that even p results in net helicity nonflip and odd p in net helicity flip.

The Gribov integral describes the two-body scattering amplitude as a two-dimensional phase space integral in the exchange plane perpendicular to the relative momentum of the incoming hadrons. The cut expression contains the kernel $K(s,\underline{k}_1,\underline{k}_2,\underline{k})$ which is the essential difference between our approach and the absorption model. The correlation kernel is parameterized as

$$K^{m(p)}(s,\underline{k}_1,\underline{k}_2,\underline{k}) = \lambda_{cut}^{m(p)}(\underline{k}) \; \exp\left[-c(s)^{m(p)}(\underline{k}_1 - \underline{k}_2)^2\right]$$

where $\lambda_{cut}^{m(p)}$ is the scale factor. This results in the helicity nonflip cut (note that the cut consists of nonrotating and

rotating parts)

$$T^0_{cut}(s,|t|) = -\frac{\beta^0_R(0,s)\ \beta^0_P(0,s)\ \lambda^0_{cut}(|t|)}{2\sqrt{\pi}\ \left(\lambda^0_R(s)+4c^0(s)+\lambda^0_P(s)\right)}$$

$$\times\ \exp\left[-\frac{\lambda^0_R(s)\ \lambda^0_P(s)+c^0(s)\left(\lambda^0_R(s)+\lambda^0_P(s)\right)}{\lambda^0_R(s)+4c^0(s)+\lambda^0_P(s)}\ |t|\right]$$

We set for the cut amplitude:

$$T^0_C(|t|) = \xi^0_C\ \exp\left|-\psi^0_C|t|\right|\ \exp\left[i\left(\phi^0_C(0)+\Phi^0_C|t|\right)\right]$$

The helicity flip* cut again consists of non-rotating and rotating parts. We write

$$T^1_{cut}(s,|t|) = -(|t|)^{\frac{1}{2}}\frac{\beta^1_R(0,s)\ \beta^0_P(0,s)\ \lambda^1_{cut}(|t|)\left(\lambda^0_P(s)+2c^1(s)\right)}{2\sqrt{\pi}\ \left(\lambda^1_R(s)+4c^1(s)+\lambda^0_P(s)\right)}$$

$$\times\ \exp\left[-\frac{\lambda^1_R(s)\ \lambda^0_P(s)+c^1\left(\lambda^1_R(s)+\lambda^0_P(s)\right)}{\lambda^1_R(s)+4c^1(s)+\lambda^0_P(s)}\ |t|\right]$$

$$= \xi^1_C\ \exp\left[-\psi^1_C\ |t|\right]\ \exp\left[i\left(\phi^1_C(0)+\Phi^1_C|t|\right)\right]$$

---

*The helicity flip poles possess an additional angular momentum factor

$$\left(\frac{|t|}{4\,m_{N^2}}\right)^{\frac{1}{2}}$$

and different residues and correlation parameter.

and the Regge-energy dependence is given by

$$\beta^{0,1}_{R,P}(s) = \hat{\beta}^{0,1}_{R,P}\, \alpha_{R,P}(0) - 1$$

$$\lambda^{0,1}_{R,P}(s) = \hat{\lambda}^{0,1}_{R,P} + \alpha'_{R,P}\, \ell n\, s - \frac{1}{2}\, i\pi\, \alpha'_{R,P}$$

E. Observables

The differential cross section, with our normalization factor N = 1 is defined as

$$\frac{d\sigma}{d|t|} = (|T^0|^2 + |T^1|^2) \quad ,$$

and the polarization of the recoil nucleon produced in a $0^- \frac{1}{2}^+ \to 0^- \frac{1}{2}^+$ reaction is

$$P(t) = \frac{2\pi\ \mathrm{Im}\ (T^0\ T^{1*})}{pq\ d\sigma/d|t|}$$

where q and p are the c.m. three momenta of the incident and scattered pions respectively.

3. Discussion and Results

3.1 Vector Exchange

A. Helicity nonflip amplitude

In the cut-pole Argand diagram (fig. 2) the correlation parameter c delays the critical point in $|t|$ (180° line) at which cut and pole are completely out of phase, until a more favourable cut modulus ratio is reached. The cut reverses the pole's anticlockwise rotation, moving the polarization zero out in $|t|$. Figure 3 shows the Argand diagram for continuous $|t|$ values. The real correlation model is in perfect

agreement with the amplitude analysis ([8]). This is again to be compared with the traditional c = 0 absorption model. For comparison we show the pole amplitude corrected by the correlated and uncorrelated cut. Away from $|t| = 0$ the polarization is determined by the relative 'velocity'

$$\Phi_C^0 - \Phi_R^0 = \Delta \Phi_{CR}^{00}$$

with which $T_C^0(|t|)$ rotates through the Argand diagram relative to $T_R^0(|t|)$. In the c = 0 model the cut rotates slowly with $\Phi_C^0 \sim 5^o$ per unit in $|t|$ compared with the fast $\Phi_R^0 \sim 72^o$ pole. Thus, pole and cut are already completely out of phase at small $|t|$. From this point the anticlockwise rotation of $T_{tot}^0(|t|)$ increases. The helicity flip pole phase remains virtually unaffected in the region $0.0 \lesssim |t| \lesssim 0.35$ $(GeV/c)^2$. The phase difference $\Delta_{tot}\phi^{10}(|t|)$ between the two helicity amplitudes changes sign from positive to negative when the relative phase between helicity nonflip cut and pole passes through 180^o. We find, due to the large trajectory slope of the pole for $|t|=0.075$ $(GeV/c)^2$ that $\alpha_{cut}^0(|t|) > \alpha_{pole}^0(|t|)$. Although $\alpha_{tot}(0) < \alpha_{pole}(0)$ we find already for small $|t|$, $\alpha_{tot}(|t|) > \alpha_{pole}(|t|)$. A real correlation model with moving effective Pomeron with real part at $|t| = 0$

$$\phi_{el}^{*0} \neq 90^o , \quad \alpha_{el}^{*\prime} \neq 0 , \quad \mathrm{Re}\, c^0 \neq 0 , \quad \mathrm{Im}\, c^0 = 0$$

provides a good-description of the helicity nonflip isovector amplitude.

B. Helicity Flip Amplitude

In fig. 4 we draw the Argand diagram for the helicity flip pole plus the correlated cut and compare with uncorrelated cut.

We divide the momentum transfer of the helicity flip amplitude into two regions: above and below $|t| = |t_0|$ where $\alpha_R = 0$. This amplitude shows Regge behaviour for $|t| \lesssim |t_0|$. This is not established for $|t| \gtrsim |t_0|$ and might be violated. One can extract both helicity isovector amplitudes for $|t| \gtrsim |t_0|$ from inelastic differential cross-section and elastic polarization data alone. The symmetric part of the elastic polarization for $\pi^{\pm}p$ is

$$P^{sym}(|t|) \sim \frac{4\ \mathrm{Im}\ {}^0T^{*0}_{el}\ {}^1T^{*1}_{tot}}{\frac{d\sigma^+}{d|t|} + \frac{d\sigma^-}{d|t|}}$$

$$= 4\frac{|{}^1T^{*0}_{el}||{}^1T^{1}_{tot}|\ \sin\left(\Delta^{01}\phi^{*01}_{el,tot}(|t|)\right)}{\frac{d\sigma(\pi^+p)}{d|t|} + \frac{d\sigma(\pi^-p)}{d|t|}}$$

with

$$\Delta^0\,{}^1\phi^{*0}_{el,tot}(|t|) = {}^0\phi^{*0}_{el}(|t|) - {}^1\phi^{1}_{tot}(|t|) \quad .$$

The left upper indices 0,1 stand for isoscalar and isovector exchange respectively.

On the basis of the ${}^0T^{*0}_{el}(|t|)$ model, the phase of the helicity flip isovector amplitude can be determined. It is constrained by

$$\left|\ {}^1T^{1}_{tot}(|t|)\ \right| \lesssim \frac{d\sigma(\pi^-p \to \pi^0 n)}{d|t|} \quad .$$

Switching the cut off produces the double zero structure in $\pi^{\pm}p$ polarization ([10]), although the rise of the theoretical curve at large $|t|$ remains weak. Setting c equal to zero produces an elastic

(10) M. Borghini et al., Phys. Letts. 31B (1970) 405.

polarization reminiscent of the traditional weak cut absorption model [11] To provide a simultaneous description of elastic $\pi^{\pm}p$ [10] and inelastic $\pi^{-}p \to \pi^{o}n$ polarization [8,12,13] we choose the helicity flip shower factor λ^{1}_{cut} such that for $|t| \gtrsim 0.6$ (GeV/c)^2 the destructive tendency of the cut is reversed

$$\lambda^{1}_{cut} = (\lambda_1 + \lambda_2 |t|) \exp(\lambda_1 + \lambda_2 |t|) |t| \quad .$$

The imaginary part of the helicity flip amplitude is prevented from becoming negative, fig. 5. The parameterization of λ^{1}_{cut} plus correlation parameter c produces an excellent quantitative fit for the polarization of $\pi^{-}p \to \pi^{o}n$ (fig. 6a) and a qualitative description of $\pi^{\pm}p$ elastic scattering, fig. 6b. This shows mirror symmetry out to $|t| = 2$ (GeV/c)^2 without a crossover at NWSZ. The describing of both $\pi^{-}p \to \pi^{o}n$ polarization and $\pi^{\pm}p$ polarization has always posed a problem More elaborate models for the Pomeron [14] show, for inelastic pion-nucleon charge exchange, a deep negative dip, or polarization zero too early in $|t|$, reminiscent of conventional absorption, fig. 7.

The differential cross section is shown for 6 GeV/c and 200 GeV/c in fig. 3 [15]. The effective trajectory [16] of 6 GeV/c and 200 GeV/c is shown in fig. 9. The weak energy dependence of the inelastic polarization, fig. 6a, reflects a stable crossover position.

---

(11) S. A. Adjei et al., Annuals of Phys. 75 (1973) 405.
(12) P. Bonamy et al., Nucl. Phys. B52 (1973) 392.
(13) D. Hill et al., Phys. Rev. Letts. 30 (1973) 239.
(14) B. J. Hartley, G. L. Kane, Nucl. Phys. 57B (1973) 157;
G. L. Kane, A. Seidl, Rev. Mod. Phys. 48 (1976) 309.
(15) P. Sonderegger et al., Phys. Letts. 20 (1966) 75.
(16) A. V. Barnes et al., Phys. Rev. Letts. 37 (1976) 76.

3.2 The Isoscalar Exchange

The elastic ρ and A_2 absorbing amplitude is the isoscalar amplitude as extracted by amplitude analysis at 6 GeV/c ([8]). We have drawn this amplitude as T^*_{el} in the Argand diagram of fig. 10 at $|t| = 0$. The amplitude has been parameterized in Regge-pole form. Its phase of 101^o corresponds to $\alpha^*_{el}(0) = 0.878$ and its slope to $\alpha^{*\prime}_{el} = 0.6$. The bare f and Pomeron pole P are also shown. Their intercept and slope are

$$\alpha_f(0) = 0.38 \quad , \qquad \alpha_P(0) = 1.00 \quad ,$$

$$\alpha'_f = 0.85\ (\mathrm{GeV/c})^{-2} \quad , \qquad \alpha'_P = 0.25\ (\mathrm{GeV/c})^{-2} \quad .$$

Both f and P are convoluted to produce f^* and P^*. The correlated cuts are shown as fC and PC in fig. 10. Thus the T^*_{el} absorbs the Regge exchange as follows

$$T = R \otimes K \otimes f + R \otimes K \otimes P + R \otimes K \otimes f \otimes P + R \otimes K \otimes P \otimes K \otimes P \quad ,$$

where K indicates the correlation kernel which rotates the amplitude clockwise. In the case of the Pomeron-Pomeron cut we have

$$T_{P \otimes P}(|t| = 0) = \xi^{00}_{P \otimes P} \exp\left[i\, \phi^{00}_{P \otimes P} \right]$$

The modulus

$$\xi^{00}_{P \otimes P} = -i \left\{ (2\sqrt{\pi})^{-1} \lambda^0_{cut} \beta^0_P \beta^0_P (s/s_0)^{2\alpha_P(0)-2} \right\}$$

$$\times \left\{ \left[2\left(\mathrm{Re}\ \lambda^0_P + \alpha'_P \ln (s/s_0)\right) + 4\mathrm{Re}\left(c^0_{1P \otimes P} + c^0_{2P \otimes P} \ln (s/s_0)\right) \right]^2 \right.$$

$$\left. + \left[4\ \mathrm{Im}\left(c^0_{1P \otimes P} + c^0_{2P \otimes P} \ln (s/s_0)\right) - \pi\alpha'_P \right]^2 \right\}^{-\frac{1}{2}} \quad .$$

The phase angle

$$\phi^{00}_{P\otimes P} = 1-\alpha_P(0) - \text{arctg}\left\{\left[4\ \text{Im}\left(c^0_{1P\otimes P} + c^0_{2P\otimes P}\ \ell n\ (s/s_0)\right) - \pi\alpha'_P\right]\right.$$

$$\left.\times\left[2\left(\text{Re}\ \lambda^0_P + \alpha'_P\ \ell n\ (s/s_0)\right) + 4\ \text{Re}\left(c^0_{1P\otimes P} + c^0_{2P\otimes P}\ \ell n\ (s/s_0)\right)\right]^{-1}\right\}$$

We give in Table 1 the parameter values which lead to a consistent description of f^*, P^*, compatible with

$$\alpha(\pi^{\pm}p) = \text{Re}\ T^*_{el}(s,0)\Big/\text{Im}\ T^*_{el}(s,0)$$

and $\sigma_{tot}(\pi^{\pm}p)$ and T^*_{el} with the amplitude analysis ([17]), figs. 11a, 11b.

Full eikonalization will dampen the sharp rise of our theoretical curve. We leave the correlation parameter c purely real but energy-dependent. To obtain the energy dependence of f^* and P^* we use the energy phase relation for $|t| = 0$. Since $c^0_2\ \ell n\ (s/s_0)$ cancels the energy dependence in the cut denominator, the power behaviour of cut and pole plus cut corresponds to their phase behaviour

$$P^* = i(s/s_0)^{\alpha_{P^*}(0)-1}\,\beta^0_{P^*}(0)\ \exp\left[i\frac{1}{2}\pi\left(1-\alpha_{P^*}(0)\right)\right]\ ,$$

$$f^* = -2(s/s_0)^{\alpha_{f^*}(0)-1}\,\beta^0_{f^*}(0)\ \cos\left\{\pi\alpha_{f^*}(0)/2\right\}\ \exp\left[-i\pi\alpha_{f^*}(0)/2\right]\ ,$$

and we obtain for the effective f^* and P^* intercepts respectively

$$\alpha_{P^*}(0) = 1.1 \quad \text{and} \quad \alpha_{f^*}(0) = 0.63\ ,$$

giving the effective $s^{-0.37}$ power fall-off due to f^* and the $s^{0.1}$ rise due to P^*.

(17) D. Bogert et al., Phys. Rev. Letts. 31 (1973) 1271.

3.3 Tensor Exchange

By setting the correlation kernel equal to one (i.e., $c^0 = 0$) in the Gribov integral we obtain weak cut absorption. The same problems occur here as with vector exchange. The cut model accelerates the anti-clockwise rotation of the pole. We again introduce a correlation modified cut. The correct evolution in $|t|$ of the helicity nonflip pole-cut and total amplitudes is shown in fig. 12.

A. Helicity Nonflip Amplitude

In fig. 13a we show the modulus $\left|T^0_{A_2}(|t|)\right|$ and in fig. 13b we show the phase angle $\phi^0_{A_2}(|t|)$. The real part Re $T^0_{A_2}(|t|)$ is given in fig. 13c and the imaginary part Im $T^0_{A_2}(|t|)$ is given in fig. 13d. The data are taken from amplitude analysis ([9]). In these figures we have drawn the total amplitudes obtained by the correlation modified cut. For parameter values see Table 1. Figure 13b also shows the phase obtained by cuts with increasing polarization, and with and without Regge-Regge cuts, and illustrates the amount of phase gained by introducing the correlation parameter. An additional cut strength parameter λ^o_{cut} kept within reasonable limits can help in further fine tuning. See Table 2.

B. Helicity Flip Amplitude

The $T^1_{exp}(|\bar{t}|)$ shows Regge behaviour up to $\alpha_R = 0$. Dealing with $|t| \leq \alpha_R = 0$ we employ the first of two model variants. To achieve the Regge-like behaviour we choose the correlation parameter c^1_{tensor} with the same numerical values as found in the case of vector exchange. We gradually suppress this cut with growing $|t|$ with the help of an exponential damping factor

$$\lambda^1_{cut}(|t|) = \exp\left[-\gamma|t|\right] .$$

Model Variant I results in a good fit of the modulus in fig. 14a, and a qualitative account of the Regge phase fig. 14b for $|t| \lesssim \alpha_R = 0$. The Regge-pole features of the helicity flip amplitude are preserved. The modulus is hardly affected by the cut, and the phase angle is rotated initially at $|t| = 0$ by a few degrees clockwise. The anticlockwise rotating amplitude is only very slightly accelerated. But as we see from the data ([9]), a cut which preserves the Regge-pole is bound to fail further out in $|t|$. The $T^1_{exp}(|t|)$ is somewhat puzzling, since it shows Regge behaviour only up to $\alpha_R = 0$. Beyond this point Regge behaviour is violated. We have encountered similar helicity flip amplitude characteristics in the case of vector exchange. The strong rise and fall of the elastic pion-nucleon polarization beyond the NWSZ, fig. 6b, implies that a Regge-pole-like helicity amplitude for $|t| > \alpha_\rho = 0$ is incompatible with the assumed Pomeron $\alpha'_P \neq 0$. The parameterization of the helicity flip cut scale factor $\lambda^1_{cut}(|t|)$ describes inelastic and elastic polarization of πN scattering in the range of momentum transfer for

$$0.00 \lesssim |t| \lesssim 2.00 \ (\mathrm{GeV/c})^2 ,$$

in connection with $c^{0,1}_{vector} \neq 0$.

We employ this parameterization in Model Variant II.

$$\lambda^1_{cut}(|t|) = (\lambda_1 + \lambda_2|t|) \exp(\gamma_1 + \gamma_2|t|) \ |t| .$$

This parameterization converts the destructive cut around $|t| = 0.45$ $(\mathrm{GeV/c})^{-2}$ into a constructive one. The c^1_{tensor} assumes the same values as in Model Variant I. The cut causes the phase $\phi^1_{tot}(|t|)$ in fig. 14b to "swing" around the linear rising phase of $\phi^1_R(|t|)$ giving a good fit to $\phi^1_{exp}(|t|)$. Real and imaginary parts are drawn in figs. 14c, 14d.

Regge-violating behaviour of helicity flip amplitudes beyond $\alpha_R = 0$ is not atypical, and has to be accounted for by models describing regions not too small in $|t|$. We have plotted in fig. 15a the differential cross section and in fig. 15b the polarization for $\pi^- p \to \eta n$. The polarization data have been taken at 5.0 GeV/c ([12]) and at 8.0 GeV/c ([18]), and averaged.

Once the helicity flip amplitude has been fitted to the amplitude analysis one can see that a negative real c^0 describes the shape of the polarization. By increasing the magnitude of the parameter, see Table 3, the theoretical polarization curve is shifted in the positive region of the diagram. The data of the differential cross section ([9]). take account of the branching ratio

$$R_\gamma = \Gamma(\eta \to \gamma) / \Gamma_{tot}(\eta) = \frac{1}{3} \quad .$$

4. Conclusion

We have successfully described phase and energy dependence of vector and tensor exchange plus polarization and rising cross sections. The cross-over position shows only weak energy dependence. Conventional absorption rotates vector and tensor exchange anticlockwise. Our approach, using correlated Reggeon exchange, reverses this trend. Regge-Regge cuts make our fits quantitative.

Further work indicates that a full implementation of the Regge-Gribov scheme with non-planar couplings may ultimately describe the phase and energy behaviour of all two-body reactions.

---

(18) SACLAY-ORSAY Collaboration, Nucl. Phys. B16 (1970) 335.

Acknowledgments

We wish to thank A. B. Kaidalov, A. Krzywicki and H. Høgaasen for helpful discussions and correspondence on this work. One of us, P. K. wishes to thank Professor Sidney Drell for his kind hospitality and the Deutscher Akademischer Austauschdienst for their support through a NATO fellowship.

This work was supported by the Department of Energy under contract DE-AC03-76SF00515.

Table 1. Parameter Values

Parameter Type	Exchange								Units
	P		f		ρ		A_2		
	Nonflip	Flip	Nonflip	Flip	Nonflip	Flip	Nonflip	Flip	
$\alpha(0)$	1.00		0.38		0.52		0.3		
α'	0.25		0.85		0.804		0.75		(a)
β	5.14	-	19.834	-	0.431	2.348	0.236	2.07	(b)
λ	2.20	-	1.58	-	4.99	1.99	1.99	1.99	(a)
Rec_1	-0.685	-	0.046	-	-0.685	-1.0	-0.75	-1.0	(a)
Imc_1	-	-	-	-	-	-1.0	-	-1.0	(a)
Rec_2	-0.1225	-	-0.275	-	-0.1225	-	-	-	(a)
Imc_2	-	-	-	-	-	-	-	-	(a)
λ_{cut}	0.5	-	1.64	-	1.00	-	1.25	-	(a)
γ	-	-	-	-	-	-	-	2.44	
λ_1	-	-	-	-	-	1.0	-	2.2	(a)
λ_2	-	-	-	-	-	-1.8	-	-4.84	(a)
γ_1	-	-	-	-	-	2.5	-	2.5	
γ_2	-	-	-	-	-	-1.0	-	-3.0	(a)
s_0	1.00								(a)

(a) $(GeV/c)^{-2}$

(b) $\frac{(mb)^{\frac{1}{2}}}{GeV/c}$

Table 2. Dependence of Helicity Nonflip Tensor Phase

On Various Cut Parameter Values [a]

Curve Label		$c^0_{tensor}(GeV/c)^{-2}$	$\alpha^{*\prime}_{el}(GeV/c)^{-2}$	δ^{*0}_{el}	λ^0_{cut}
	a	0	0	90^o	1.0
Pole	b	0	0.6	101^o	1.0
plus	c	-0.75	0.6	101^o	1.0
Cut	d	-0.75	0.6	101^o	1.0
	e	-0.75	0.6	101^o	1.25

[a] fig. 13b

Table 3. Dependence of Polarization of $\pi p^- \to \eta n$

On Various Cut Parameter Values [a]

Curve Label	$c^0_{tensor}(GeV/c)^{-2}$	$\alpha^{*\prime}_{el}(GeV/c)^{-2}$	δ^{*0}_{el}
a	0	0	90^o
b	0	0.6	101^o
c	-0.25	0.6	101^o
d	-0.50	0.6	101^o
e	-0.75	0.6	101^o

[a] fig. 15b

Figure Captions

Fig. 1. Gribov's full double scattering amplitude with non-planar couplings: (a) unenhanced; (b) and (c) semi-enhanced; (d) fully enhanced.

Fig. 2. Cut pole Argand diagram: P is pole amplitude; - - - 180^{o} is critical 180^{o} line, where polarization zero occurs; NRC is non-rotating cut amplitude; RC is rotating cut amplitude; TC is total cut amplitude; -•-•TA is total pole + cut amplitude.

Fig. 3. Argand diagram for helicity nonflip isovector amplitude ${}^{1}T^{0}(|t|)$. Labelled divisions on curves indicate values of $|t|$. Crossover has only slight energy dependence. - - - is pole amplitude; —— is total amplitude, uncorrelated cut; --•-- is total amplitude, correlated cut; -•-• is centre points of data at 6 GeV/c; •••• is extrapolation of correlated cut to 200 GeV/c (amplitude values scaled up by factor of 10).

Fig. 4. Argand diagrams (a) for helicity flip isovector amplitude ${}^{1}T^{1}(|t|)$ for small $|t|$ values: - - - is pole amplitude; —— is total amplitude, uncorrelated cut; -•-• is total amplitude, correlated cut; (b) for large $|t|$ values on enlarged scale.

Fig. 5. Argand diagram for helicity flip isovector amplitude ${}^{1}T^{1}(|t|)$ in $0.45 \lesssim |t| \lesssim 2.00$ $(\mathrm{GeV}/c)^{2}$ region, on enlarged scale: -•-• is correlated cut with $|t|$ dependent scale factor.

Fig. 6. (a) Inelastic polarization with correlated cut: - - - is 6 GeV/c; —— is with t dependent enhancement factor 6 GeV/c; -•-• is 200 GeV/c; •••• is conventional absorptive cut with c = 0, 6 GeV/c;
(b) Elastic $\pi^{\pm}$ polarization: - - - is 6 GeV/c and -•-• is 200 GeV/c.

Fig. 7. Kane Model: —— is HK (Hartley and Kane) 6 GeV/c , and •••• is KS (Kane and Seidl) 4.9 GeV/c.

Fig. 8. Inelastic differential cross section: - - - is 6 GeV/c, and -•-• is 200 GeV/c.

Fig. 9. Effective ρ-trajectory: - - - is 6 GeV/c, and -•-• is 200 GeV/c.

Fig. 10. Argand diagram for elastic amplitude T_{el} with t = 0, at 6 GeV/c: f,P indicate bare f and Pomeron poles; fC,PC indicate correlated f and P cuts; f^*,P^* and T^*_{el} indicate cut rotated amplitudes

Fig. 11. (a) Ratio of real to imaginary part of the $\pi^{\pm}p$ elastic amplitude; (b) the σ_{tot} measured in mb up to Batavia energies.

Fig. 12. Evolution in $|t|$ of helicity nonflip pole-cut and total amplitudes: P,C is pole, cut; RP is rotating pole; NRP is non-rotating pole; RC is rotating cut; NRC is non-rotating cut; T is total amplitude.

Fig. 13. Helicity nonflip tensor exchange amplitude: (a) modulus; (b) phase; (c) real part; (d) imaginary part: ···· is pole, — — is cut, -·-· is total, and —— is uncorrelated cut.

Fig. 14. Helicity flip tensor exchange amplitude: (a) modulus; (b) phase; (c) real part; (d) imaginary part: ···· is pole, — — is cut I, -·-· is total I, --·-- is cut II and --·-·-- is total II.

Fig. 15. (a) Differential cross section of $\pi^- p \to \eta n$.
(b) Polarization for $\pi^- p \to \eta n$.
(For a,b,c,d,e curves see Table 3.)

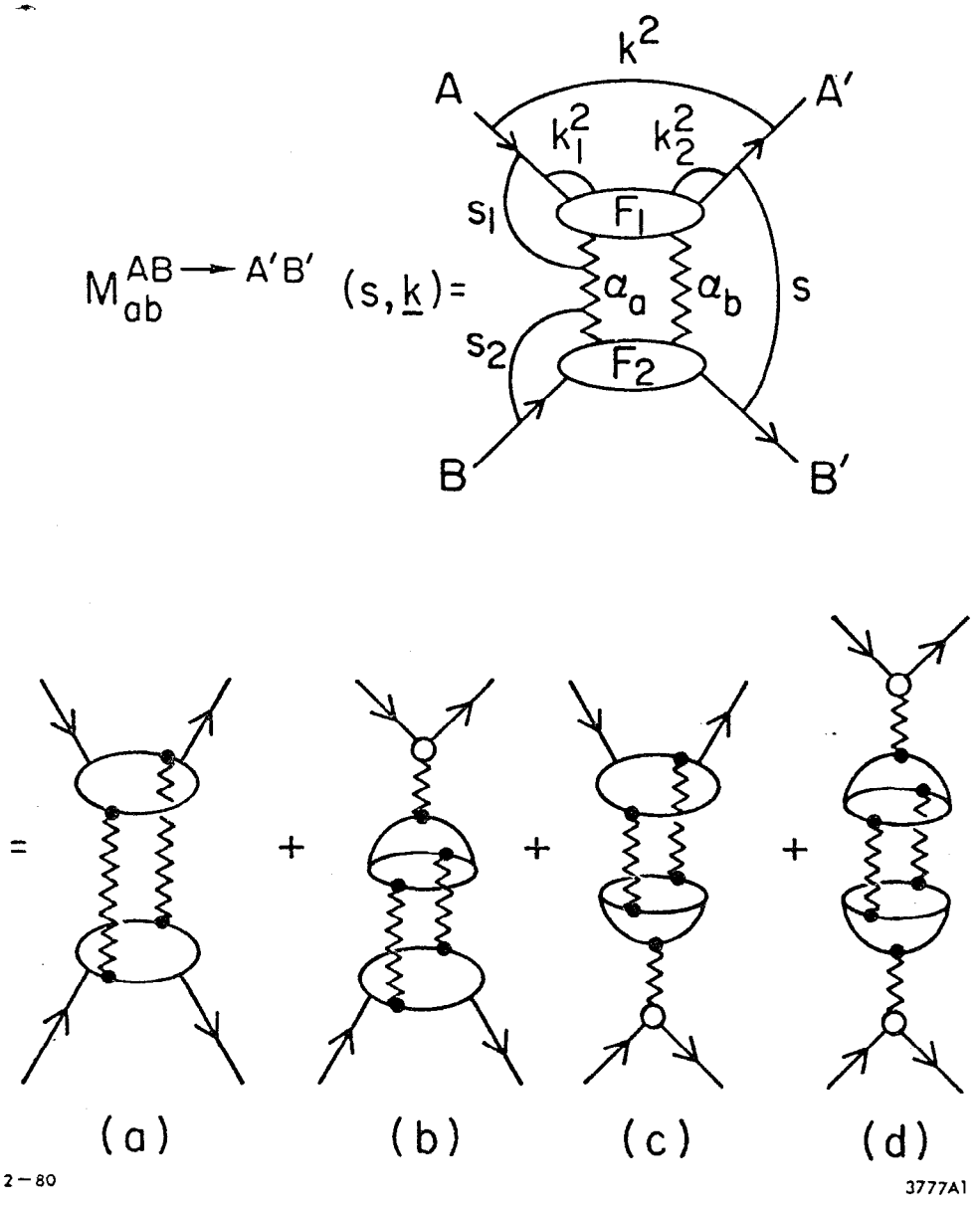
$M_{ab}^{AB \to A'B'}(s,\underline{k})=$
A
A′
B
B′
k^2
k_1^2
k_2^2
s_1
s_2
s
F_1
F_2
α_a
α_b
=
+
+
+
(a)
(b)
(c)
(d)
2-80
3777A1

Fig. 1

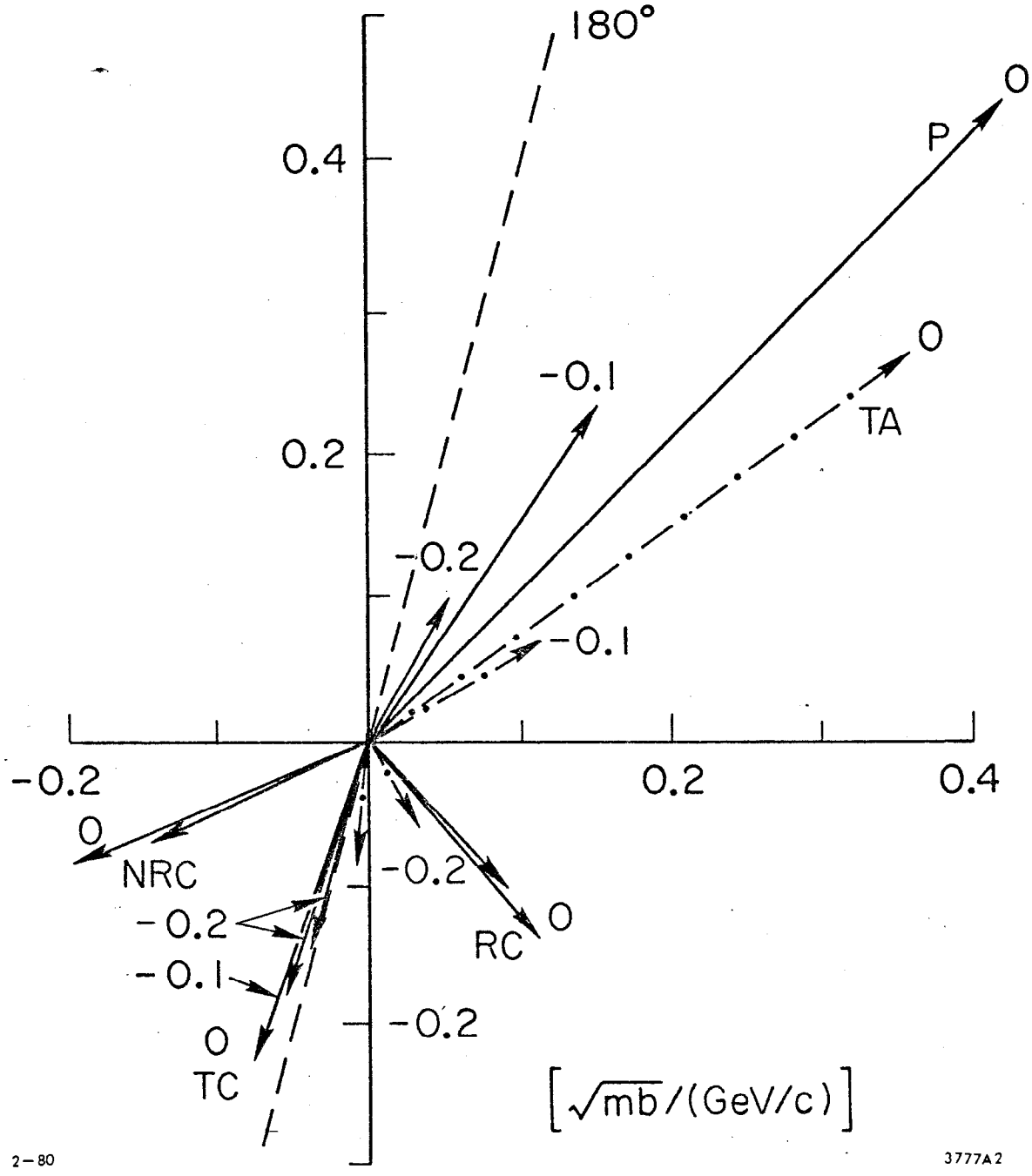
180°
0
P
0.4
0.2
-0.1
0
TA
-0.2
-0.1
-0.2
0.2
0.4
0
NRC
-0.2
-0.2
0
RC
-0.1
0
TC
-0.2
[√mb/(GeV/c)]
2-80
3777A2

Fig. 2

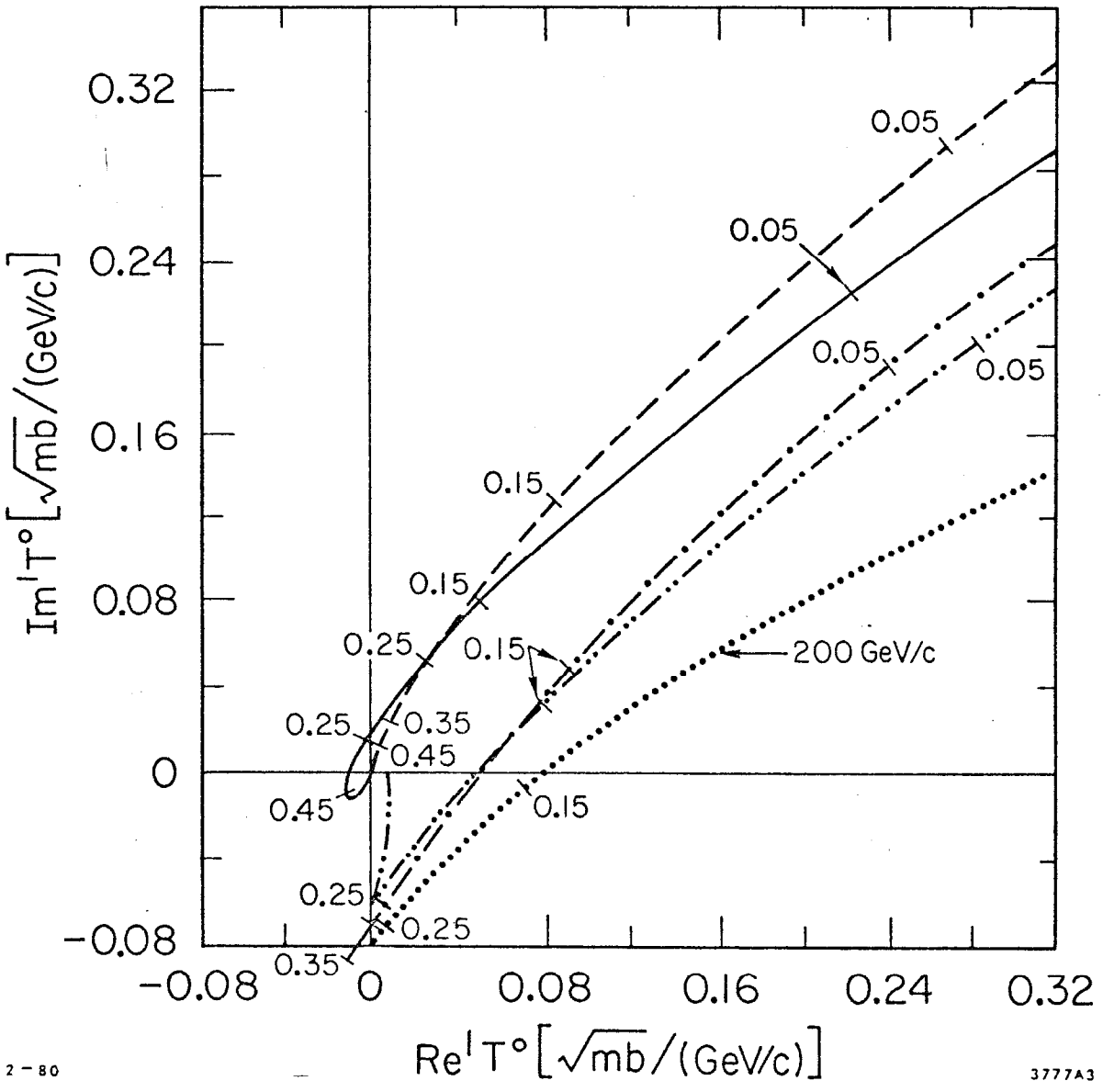
0.32
0.24
0.16
0.08
0
-0.08
-0.08
0
0.08
0.16
0.24
0.32
Im[T°] [√mb/(GeV/c)]
Re[T°] [√mb/(GeV/c)]
0.05
0.05
0.05
0.05
0.15
0.15
0.15
0.25
0.25
0.35
0.45
0.45
0.15
0.25
0.25
0.35
200 GeV/c
2-80
3777A3

Fig. 3

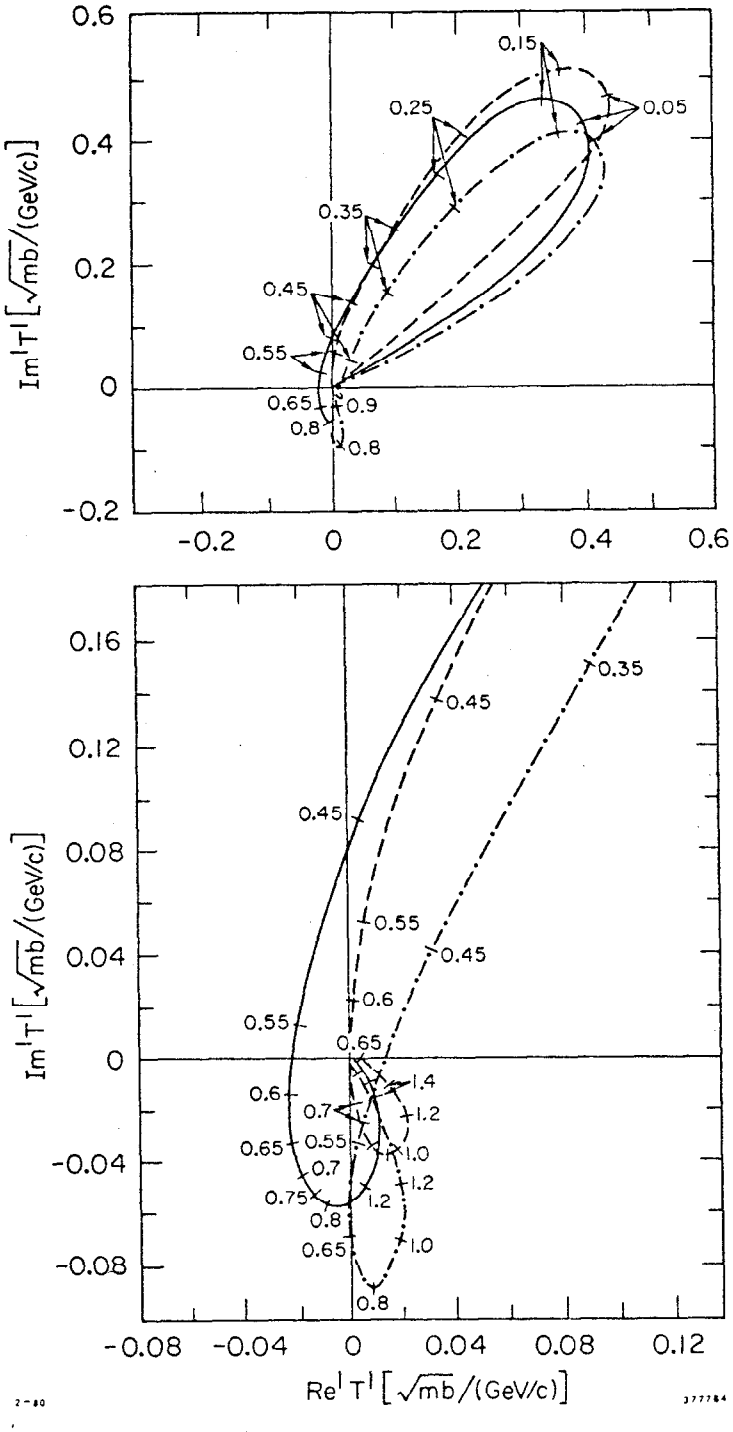
0.6
0.4
0.2
0
-0.2
-0.2
0
0.2
0.4
0.6
Im T^I [√mb/(GeV/c)]
0.15
0.25
0.05
0.35
0.45
0.55
0.65
0.9
0.8
0.8
0.16
0.12
0.08
0.04
0
-0.04
-0.08
-0.08
-0.04
0
0.04
0.08
0.12
Re T^I [√mb/(GeV/c)]
0.35
0.45
0.45
0.55
0.45
0.6
0.55
0.65
1.4
0.6
0.7
1.2
0.65
0.55
1.0
0.7
1.2
0.75
1.2
0.8
0.65
1.0
0.8

Fig. 4

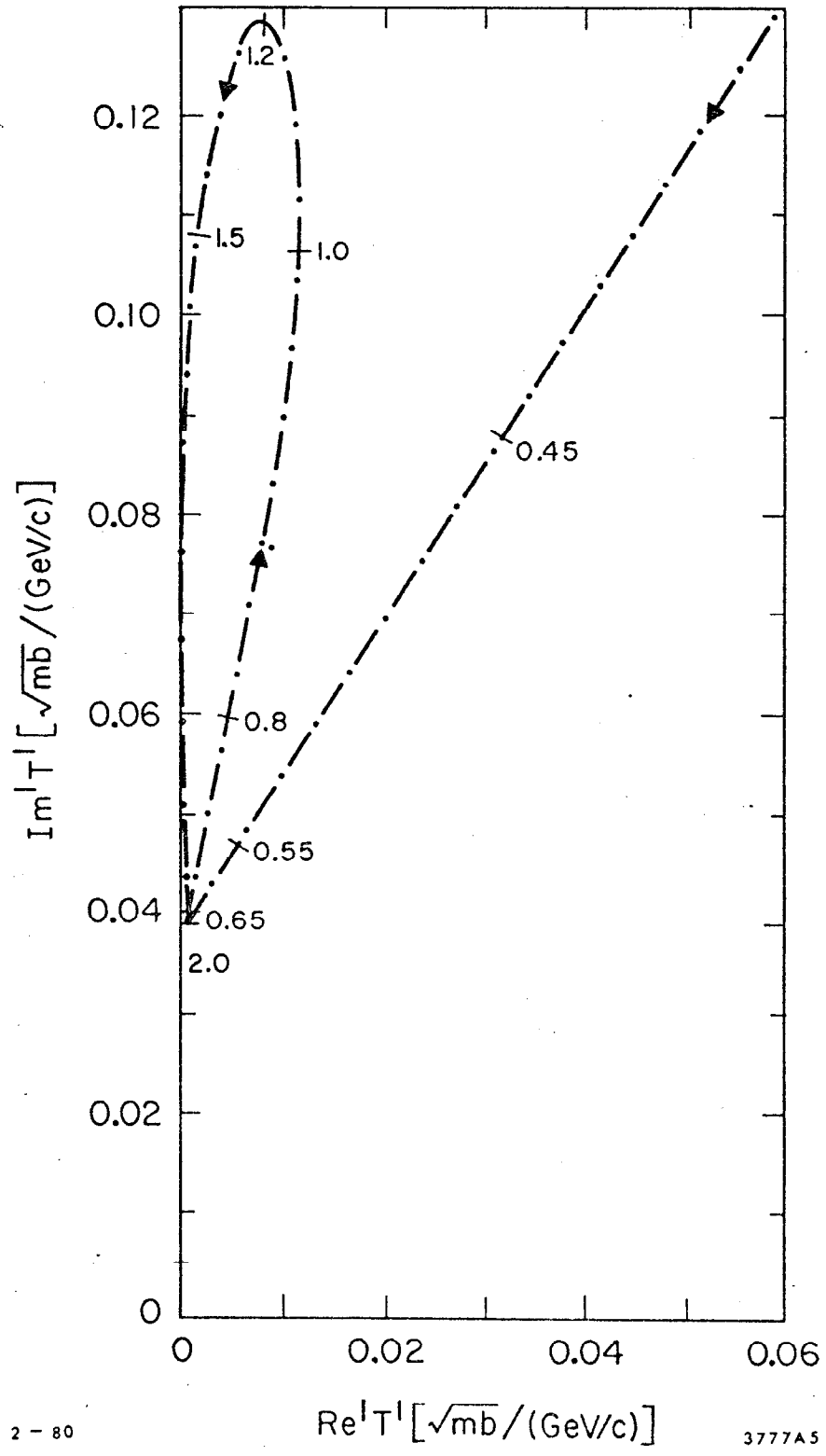
0.12
0.10
0.08
0.06
0.04
0.02
0
0
0.02
0.04
0.06
1.2
1.5
1.0
0.45
0.8
0.55
0.65
2.0
Im[T] [√mb/(GeV/c)]
Re[T] [√mb/(GeV/c)]
2 - 80
3777A5

Fig. 5

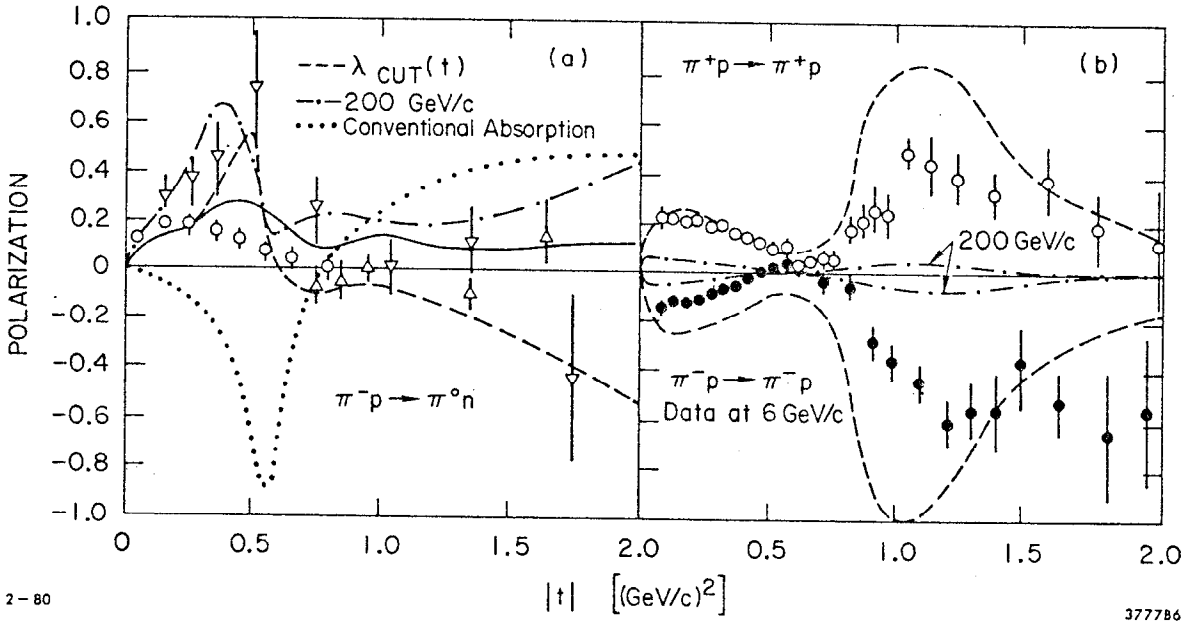
1.0
0.8
0.6
0.4
0.2
0
-0.2
-0.4
-0.6
-0.8
-1.0
POLARIZATION
---λ CUT(t)
-·-200 GeV/c
····Conventional Absorption
(a)
π⁻p→π°n
π⁺p→π⁺p
(b)
200 GeV/c
π⁻p→π⁻p
Data at 6 GeV/c
0
0.5
1.0
1.5
2.0
0.5
1.0
1.5
2.0
|t| [(GeV/c)²]
2-80
377786

Fig. 6

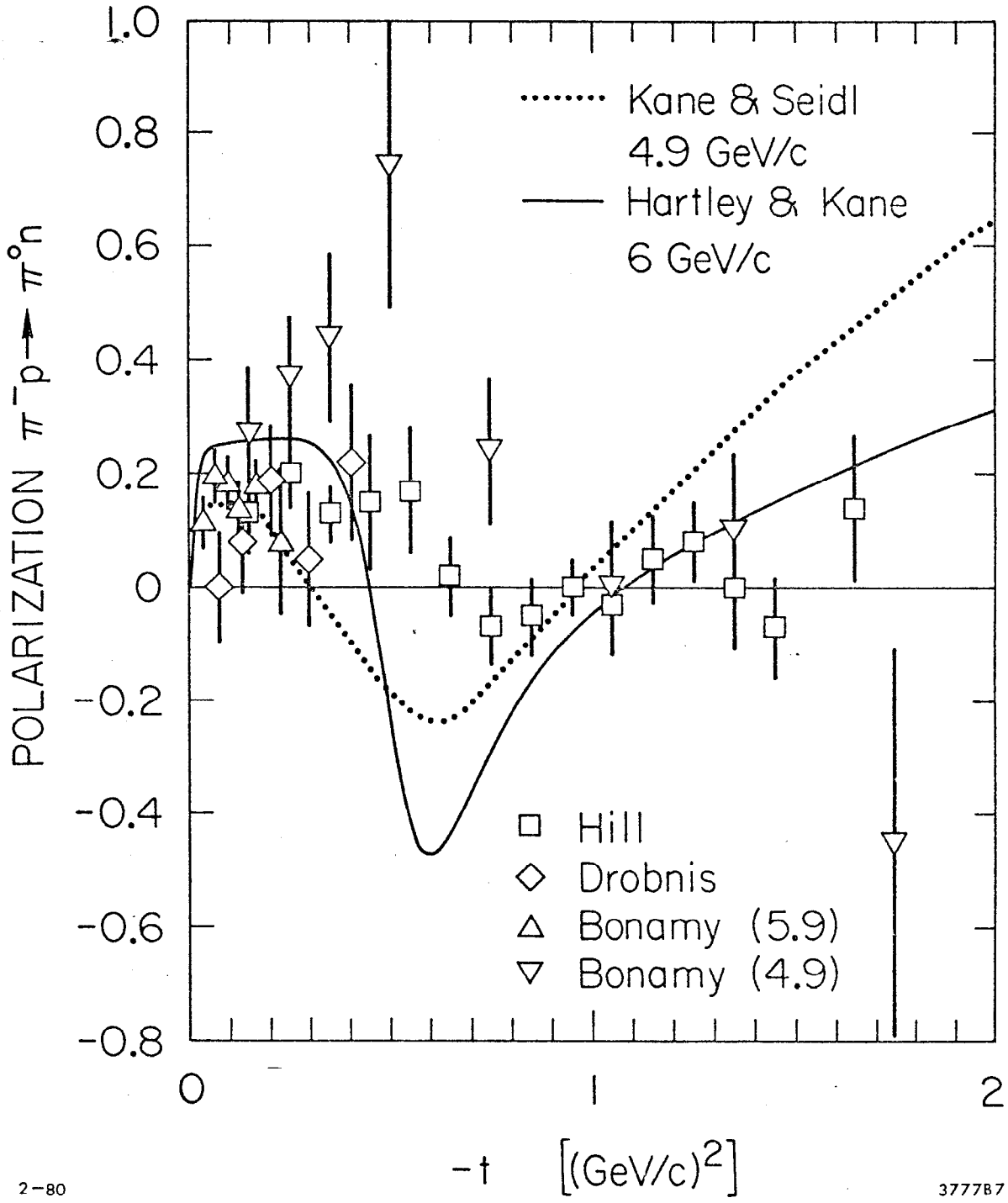
1.0
0.8
0.6
0.4
0.2
0
-0.2
-0.4
-0.6
-0.8
POLARIZATION $\pi^- p \rightarrow \pi^0 n$
Kane & Seidl
4.9 GeV/c
Hartley & Kane
6 GeV/c
Hill
Drobnis
Bonamy (5.9)
Bonamy (4.9)
0
1
2
$-t$ $[(GeV/c)^2]$
2-80
3777B7

Fig. 7

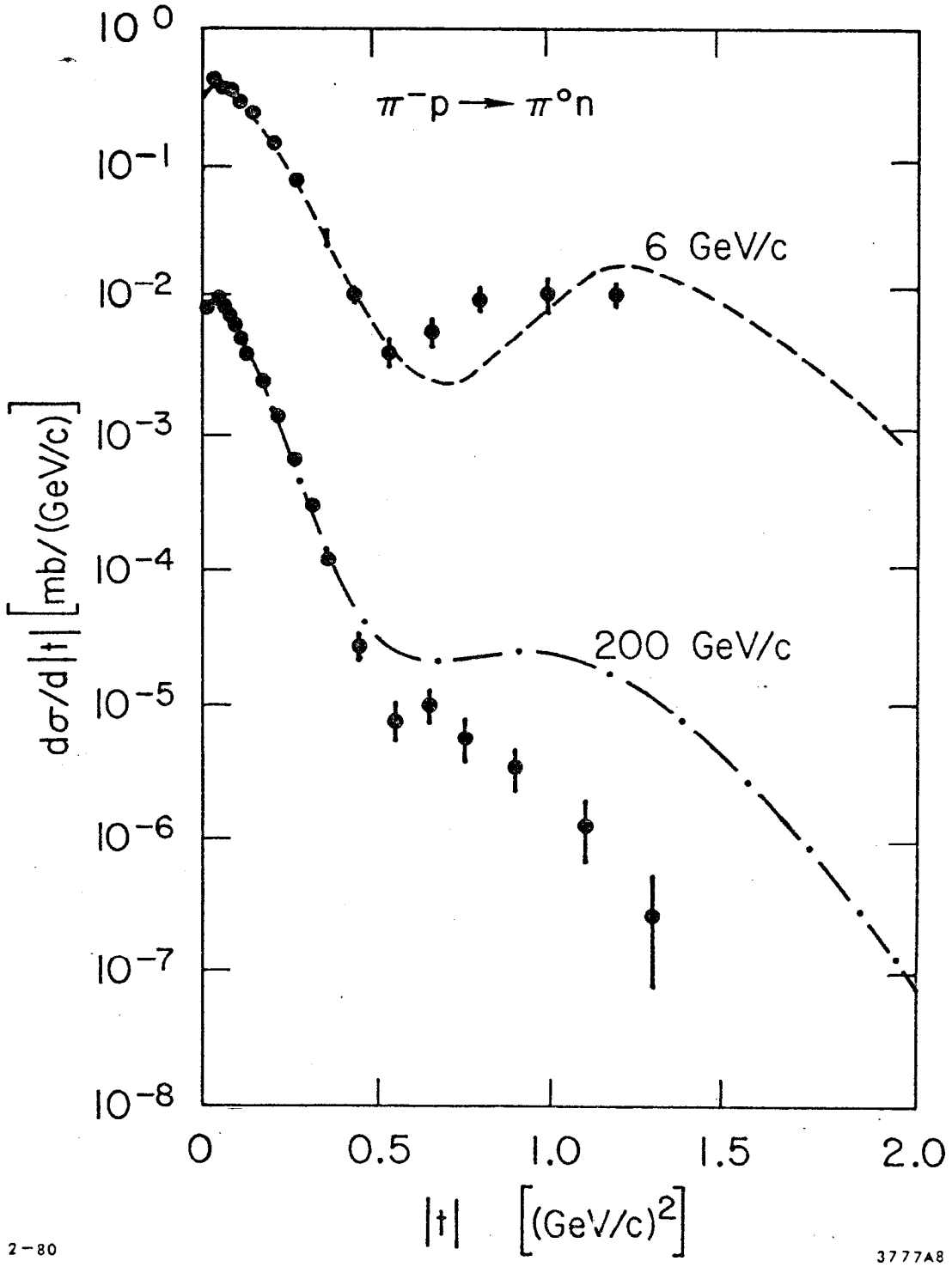
10^0
10^{-1}
10^{-2}
10^{-3}
10^{-4}
10^{-5}
10^{-6}
10^{-7}
10^{-8}
$\pi^- p \rightarrow \pi^0 n$
6 GeV/c
200 GeV/c
$d\sigma/d|t|$ [mb/(GeV/c)]
0
0.5
1.0
1.5
2.0
$|t|$ [(GeV/c)^2]
2-80
3777A8

Fig. 8

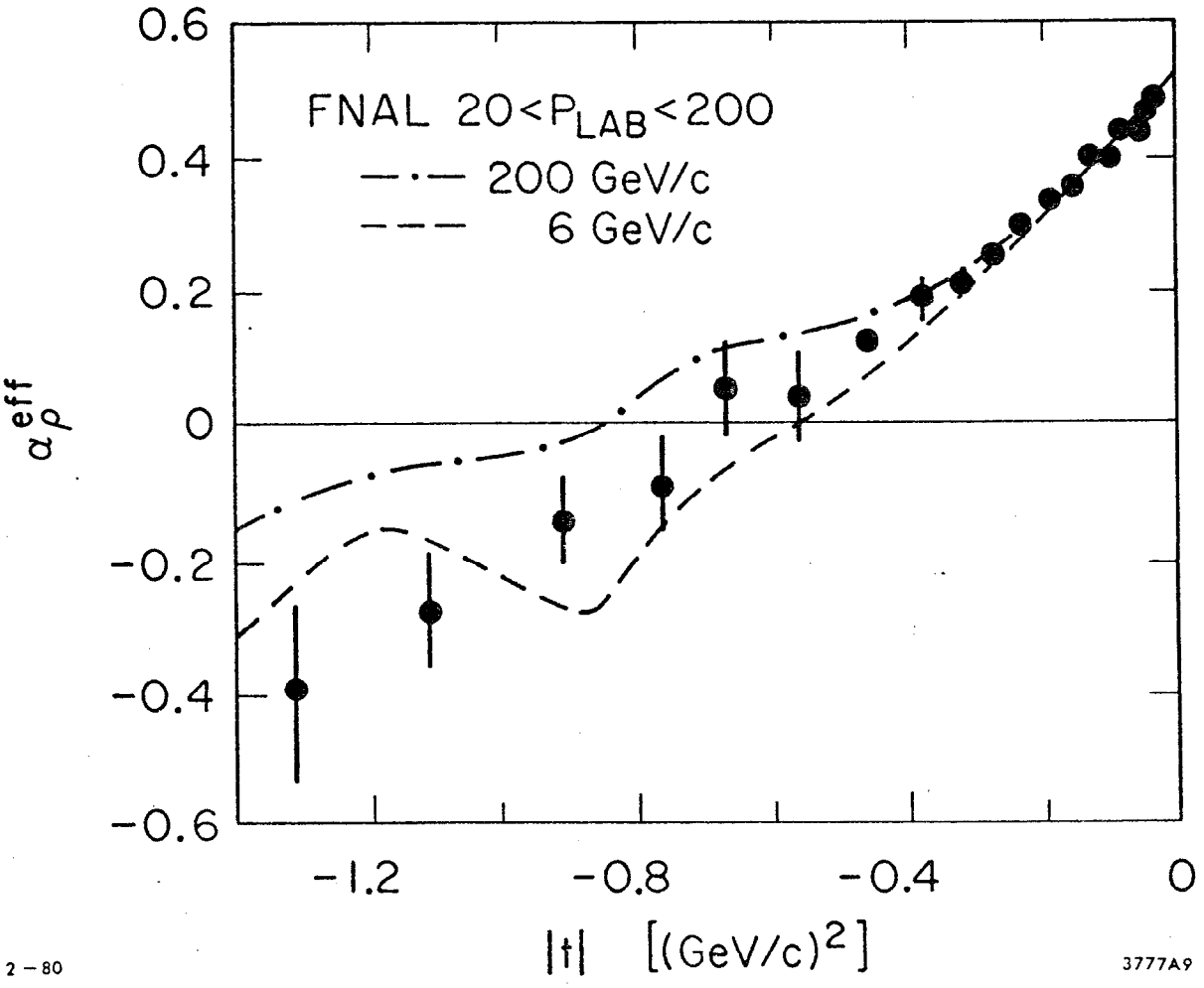
FNAL 20<P_LAB<200
200 GeV/c
6 GeV/c
0.6
0.4
0.2
0
-0.2
-0.4
-0.6
-1.2
-0.8
-0.4
0
α_ρ^eff
|t| [(GeV/c)^2]
2-80
3777A9

Fig. 9

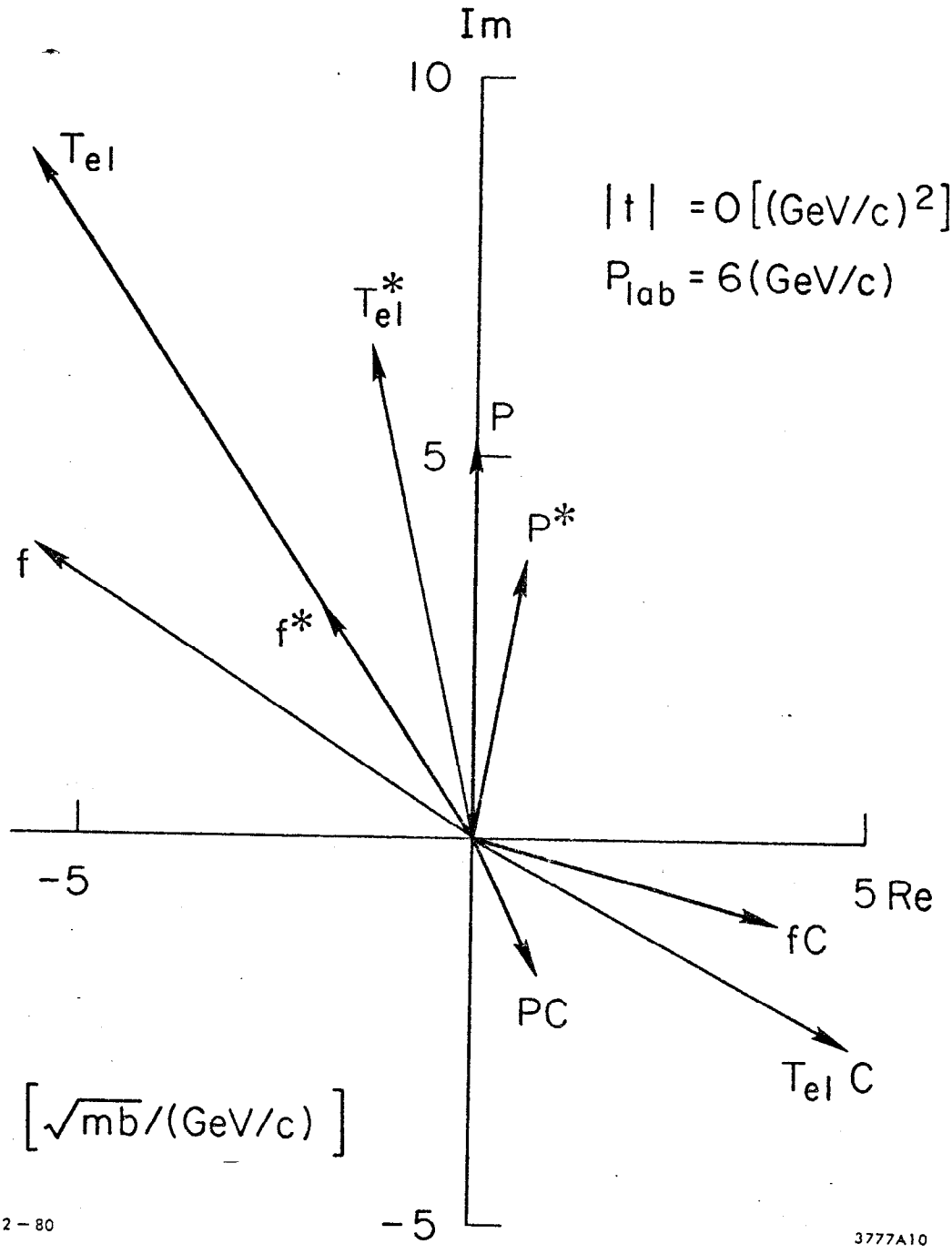
Im
10
T_{el}
$|t| = 0[(GeV/c)^2]$
$P_{lab} = 6(GeV/c)$
T_{el}^*
P
5
P*
f
f*
-5
5 Re
fC
PC
T_{el} C
$[\sqrt{mb}/(GeV/c)]$
-5
2-80
3777A10

Fig. 10

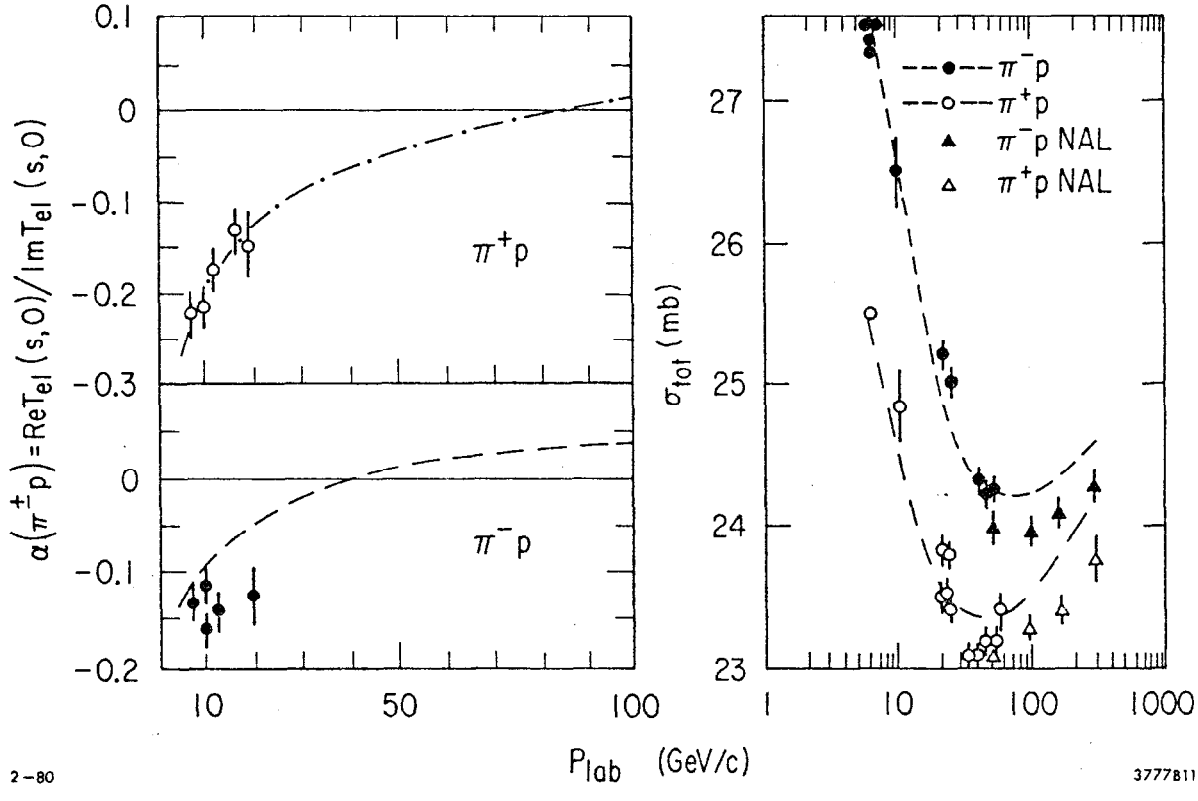
0.1
0
-0.1
-0.2
-0.3
0
-0.1
-0.2
$\alpha(\pi^{\pm}p) = ReT_{el}(s,0)/ImT_{el}(s,0)$
π^+p
π^-p
10
50
100
27
26
25
24
23
σ_{tot} (mb)
π^-p
π^+p
π^-p NAL
π^+p NAL
1
10
100
1000
P_{lab} (GeV/c)
2-80
3777B11

Fig. 11

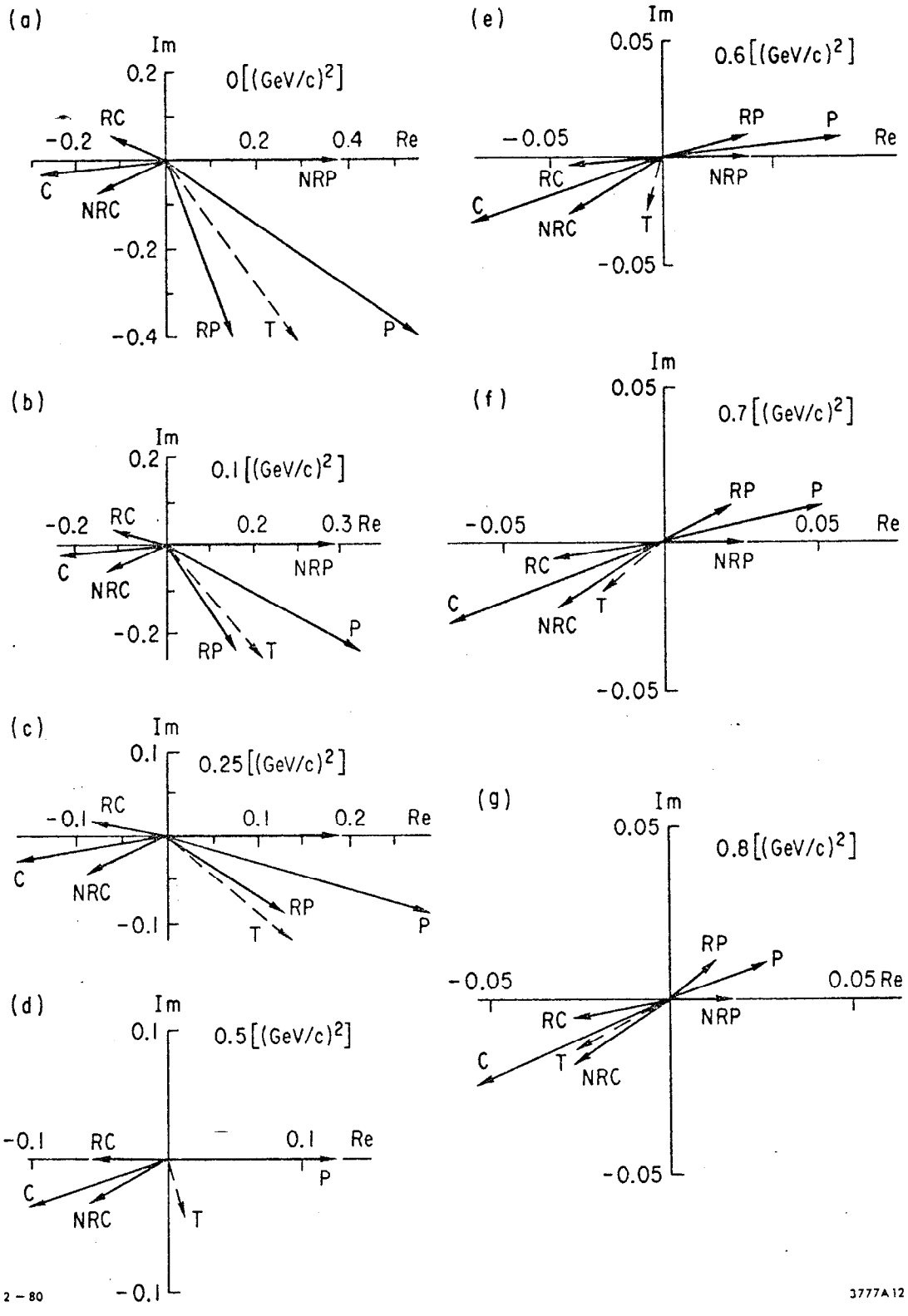
(a)
Im
0.2
0[(GeV/c)²]
RC
-0.2
0.2
0.4
Re
C
NRC
NRP
-0.2
-0.4
RP
T
P
(b)
Im
0.2
0.1[(GeV/c)²]
-0.2
RC
0.2
0.3 Re
C
NRC
NRP
-0.2
RP
T
P
(c)
Im
0.1
0.25[(GeV/c)²]
-0.1
RC
0.1
0.2
Re
C
NRC
RP
-0.1
T
P
(d)
Im
0.1
0.5[(GeV/c)²]
-0.1
RC
0.1
Re
P
C
NRC
T
-0.1
(e)
Im
0.05
0.6[(GeV/c)²]
RP
P
-0.05
Re
RC
NRP
C
NRC
T
-0.05
(f)
Im
0.05
0.7[(GeV/c)²]
RP
P
-0.05
0.05
Re
RC
NRP
C
T
NRC
-0.05
(g)
Im
0.05
0.8[(GeV/c)²]
RP
P
-0.05
0.05 Re
RC
NRP
C
T
NRC
-0.05
2-80
3777A12

Fig. 12

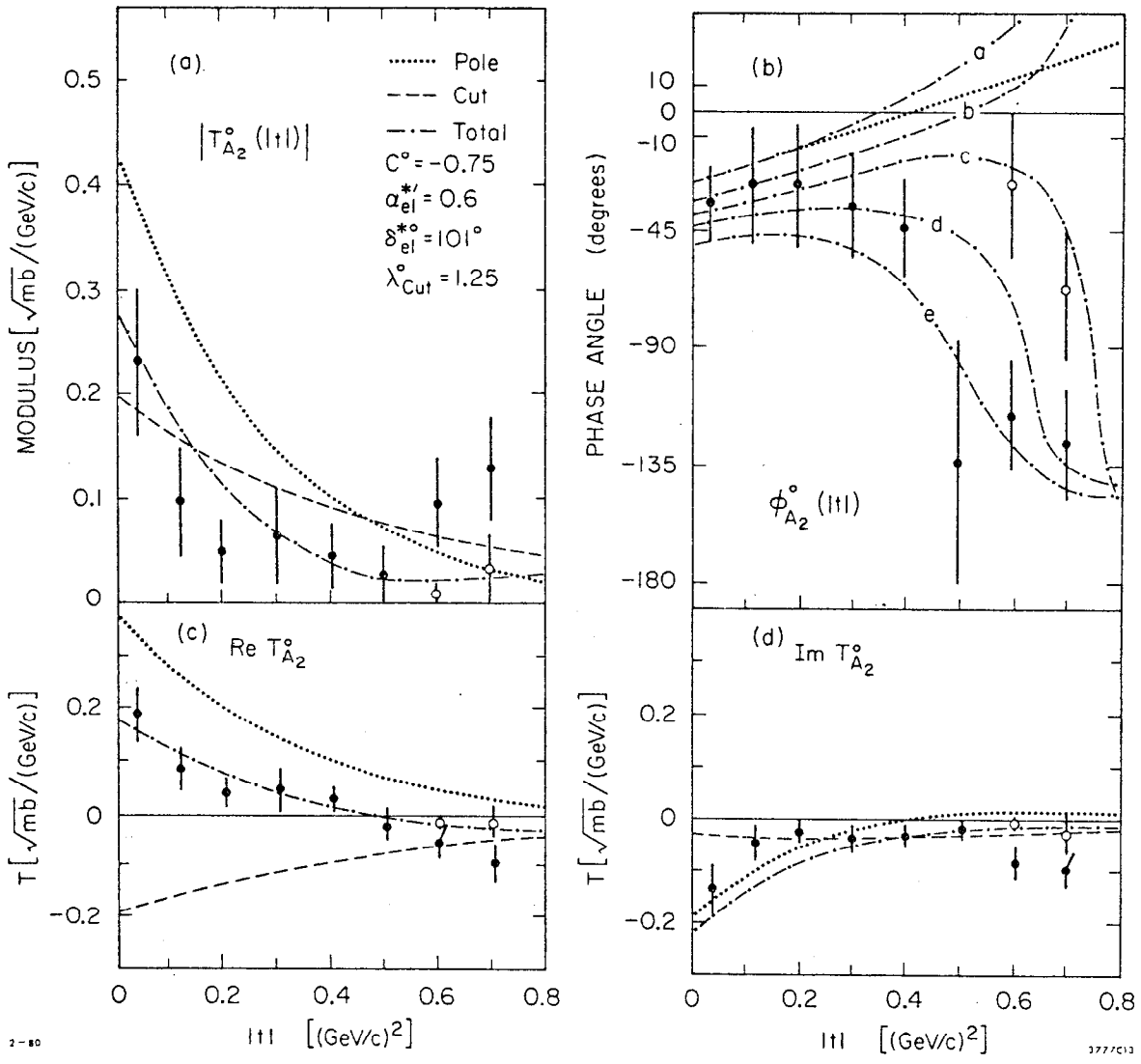
(a)
Pole
Cut
Total
$|T^{\circ}_{A_2}(|t|)|$
$C^{\circ} = -0.75$
$\alpha^{*\prime}_{el} = 0.6$
$\delta^{*\circ}_{el} = 101^{\circ}$
$\lambda^{\circ}_{Cut} = 1.25$
MODULUS $[\sqrt{mb}/(GeV/c)]$
(b)
PHASE ANGLE (degrees)
$\phi^{\circ}_{A_2}(|t|)$
a
b
c
d
e
(c) Re $T^{\circ}_{A_2}$
(d) Im $T^{\circ}_{A_2}$
$T[\sqrt{mb}/(GeV/c)]$
$|t|$ $[(GeV/c)^2]$
3777C13

Fig. 13

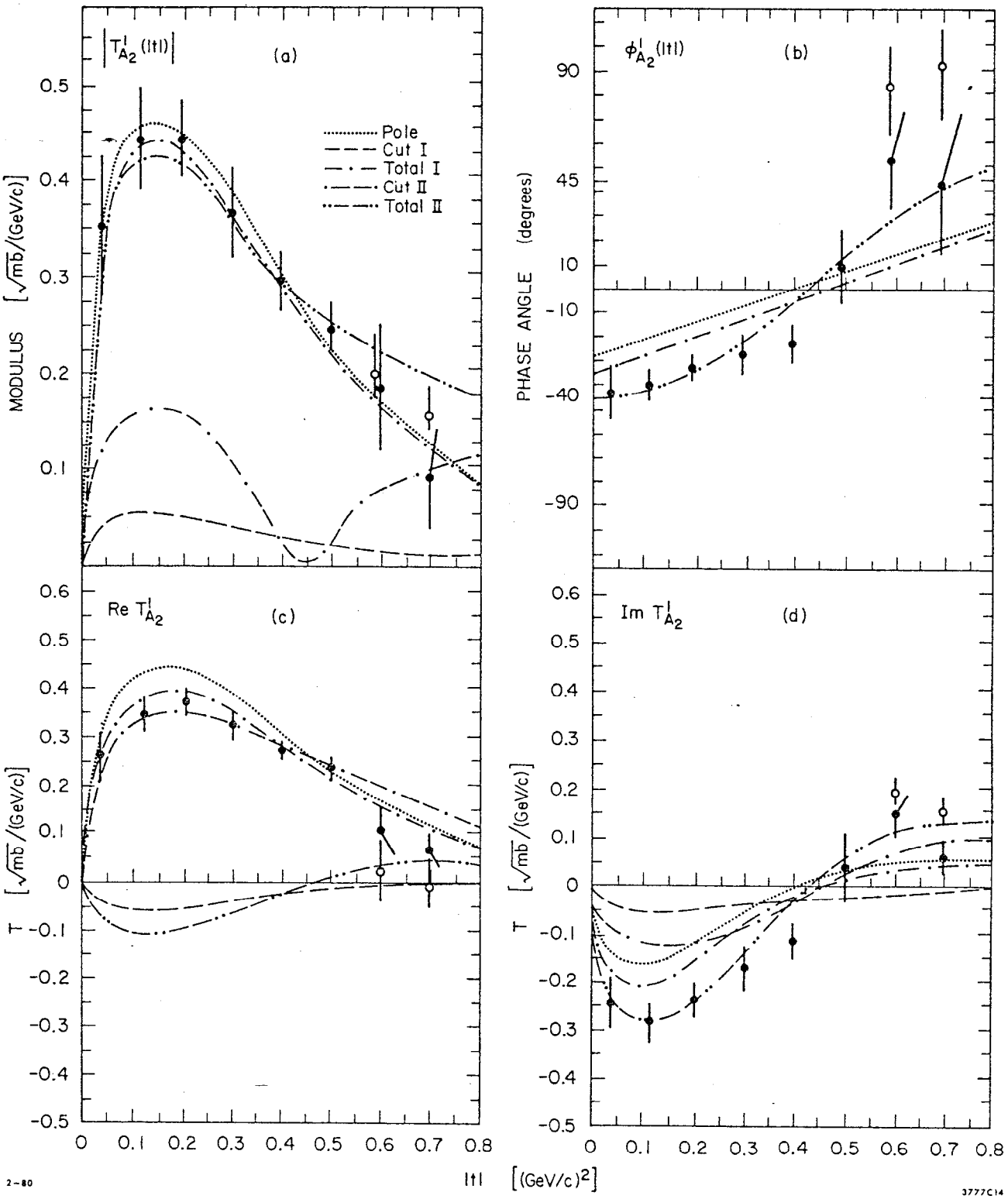
$|T^I_{A_2}(|t|)|$
(a)
Pole
Cut I
Total I
Cut II
Total II
MODULUS $[\sqrt{mb}/(GeV/c)]$
$\phi^I_{A_2}(|t|)$
(b)
PHASE ANGLE (degrees)
Re $T^I_{A_2}$
(c)
Im $T^I_{A_2}$
(d)
T $[\sqrt{mb}/(GeV/c)]$
$|t|$ $[(GeV/c)^2]$
2-80
3777C14

Fig. 14

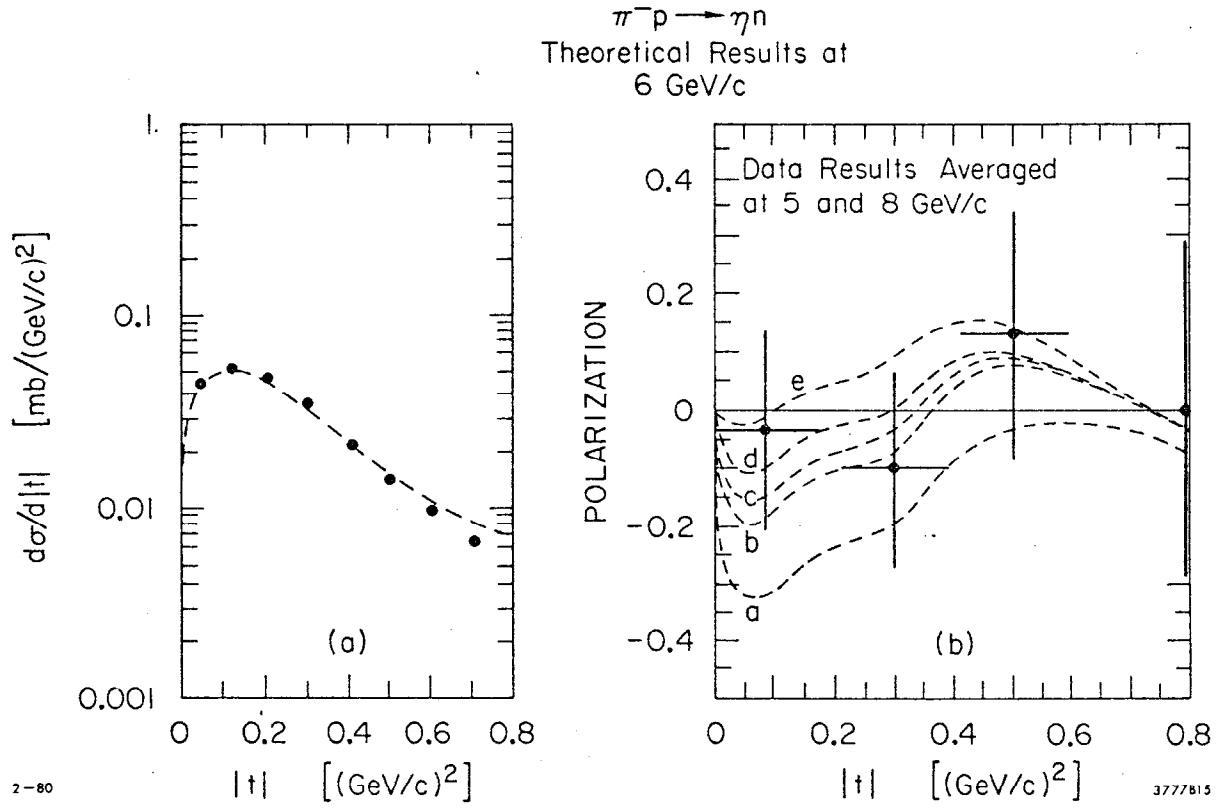
$\pi^- p \rightarrow \eta n$
Theoretical Results at
6 GeV/c
Data Results Averaged
at 5 and 8 GeV/c
$d\sigma/d|t|$ [mb/(GeV/c)^2]
POLARIZATION
|t| [(GeV/c)^2]
(a)
(b)
a
b
c
d
e
2-80
3777815

Fig. 15